

A NOVEL HETEROSTRUCTURED AgI/Ag₃BiO₃ NANOCOMPOSITE WITH ENHANCED PHOTOCATALYTIC AND STABILITY UNDER VISIBLE LIGHT

F. WANG, P. LIN, G. S. HUANG, S. Y. HU, L. CHEN, Z. SONG*

College of Chemistry, Changchun Normal University, Changchun 130032, Jilin, People's Republic of China

The AgI/Ag₃BiO₃ nanocomposites were synthesized through a two-step chemical process including the hydrothermal and the chemical bath deposition methods. The as-synthesized photocatalysts were characterized by X-ray powder diffraction (XRD), scanning electron microscopy (SEM), and PL spectra (PL) techniques. The photocatalytic degradation of AgI/Ag₃BiO₃ was investigated in detail. The results revealed that the AgI/Ag₃BiO₃ composites exhibited significantly higher photocatalytic activities than the pure AgI and Ag₃BiO₃. Additionally, the quenching investigation of different scavengers demonstrated that h⁺, •OH, •O₂⁻ reactive species played different roles in the decolorization of methyl orange (MO). Our results showed that AgI/Ag₃BiO₃ nanocomposites could be used as an effective photocatalyst.

(Received April 23, 2019; Accepted June 27, 2019)

Keyword: Hydrothermal synthesis, Degradation efficiency, Nanocomposite

1. Introduction

Recently, silver-based photocatalysts have attracted wide attention to resolve the energy crisis and environment pollution. Due to their unique structures and exhibited remarkable performances, Ag-based semiconductor photocatalysts with remarkably improved photocatalytic performance have already been reported, such as Ag₂CdI₄/AgI, AgI/Bi₅O₇I, AgI/BiPO₃, AgI/C₃N₄, AgI/TiO₂, and so on [1-6]. As a new perovskite photocatalyst semiconductor, Ag₃BiO₃ which formed from Bi₂O₃ and Ag₂O, has suitable band gap (2.04 eV) [7]. Similar to BiOX, doping AgX on alloyed compounds are expected to improve the bactericidal capacity [8-12]. However, the disinfection effects and mechanisms involved in the photocatalytic disinfection processes of binary Ag₃BiO₃ based photocatalysts have not been studied and thus required investigation.

AgX (X = Cl, Br, I) contain intrinsic antibacterial capacity and could help the separation of hole-electron pairs in the nanocomposites, Ag-based semiconductor photocatalysts has been also modified with AgX and enhanced antibacterial capacity was obtained [13-17].

Herein, this study is to fabricate AgX modified Ag₃BiO₃ composites and examine their disinfection effects. AgI/Ag₃BiO₃ nanocomposites were synthesized by a solvothermal process. The mechanisms involved in the photocatalytic disinfection system were systematically investigated and the major active species contributing to antimicrobial activity were determined.

2. Experimental

2.1. Materials

AgNO₃, Bi(NO₃)₃·5H₂O, NaOH, KI, concentrated HNO₃ and other reagents were obtained from commercial sources. Milli-Q water (resistivity >18.0 MΩ·cm) was used throughout the experiments. All the chemicals used in this work without further purification.

*Corresponding author: songzheszh@126.com

2.2. Synthesis of Ag₃BiO₃ composite

The Ag₃BiO₃ was synthesized via a hydrothermal method. At first, 3mmol of silver nitrate was dissolved in 30ml deionized water, named A solution. Then 1mmol bismuth nitric acid was added to the 10ml deionized water of 2ml concentrated nitric acid after 10min stirring at room temperature, formed B mixture. Next to B put into A forming C mixed solution on the electromagnetic stirring for 10 minutes. 2.0g sodium hydroxide was dissolved in 10ml deionized water and formed D solution. D solution was added drop by drop into the C which was in mechanical rabble in the next moment and stir for another 20min. After that, the obtained mixture transferred into a 100ml Teflon-lined stainless steel autoclave (filling degree of 70%) and heated in an oven maintained at 180 °C for 12 h, cooled to room temperature. The resulting product was washed with absolute ethanol and distilled water for several times, dried in an oven at 60 °C for 12 h and avoided light preservation for further use.

2.3. Preparation of different molar ratio of AgI/Ag₃BiO₃ sample

Preparation of AgI/Ag₃BiO₃ (mole ratio is 1:1 of AgI to Ag₃BiO₃) sample: 0.5mmol Ag₃BiO₃ (0.291g) was dispersed in 30 mL of deionized water by vigorously stirring for 30 min. Then 0.5mmol AgNO₃ (0.085g) was added in the above solution formed solution A. 0.5 mmol KI was dispersed in 30 ml deionized water formed solution B, and the solution B was added dropwise in mixture A under vigorously stirring for 15 min. The resulting precipitates were collected and washed with deionized water, and dried at 60 °C for 12 h. The AgI/Ag₃BiO₃ (mole ratio is 1:1 of AgI to Ag₃BiO₃) sample was marked as AgI/ABO-1:1. Different AgI/Ag₃BiO₃ samples were obtained by adjusting the mole ratio of AgNO₃ and KI, and the as-synthesized AgI/ABO photocatalysts were marked as AgI/ABO -3:1, AgI/ABO -5:1, AgI/ABO -7:1 and AgI/ABO -9:1, respectively. (ABO means Ag₃BiO₃).

2.4. Characterization of catalytic

The crystalline phases of composites were characterized by X-ray diffraction (XRD) using a D8-Advance with Cu K α ($\lambda=0.15406\text{nm}$) radiation. The morphologies were obtained on a Hitachi SU8000 field emission scanning electron microscope (SEM). Energy dispersive X-ray spectroscopy (EDS) was associated with SU8000 to detect the element of the as-obtained samples. The Photoluminescence spectroscopy (PL) spectra were collected on fluorescence spectrophotometer (HITACHI F-7000).

2.5. Photocatalytic experiments

The photocatalytic performance of the materials were investigated by degrading methyl orange (MO) (10mg/L) under the visible light (300W Xe lamp). In a typical approach, 50mg of the catalyst power was uniformly suspended in a 100 mL of MO aqueous solution and was maintained at 298 K via thermostatic bath. Then, the suspension was stirred in a Pyrex photoreactor under the dark environment for 20 min before irradiation which was sufficient to reach adsorption/desorption equilibrium. During irradiation, 3 ml of the suspension was drawn from the reactor every 10 min and centrifuged at 5,000 rpm for 10 min. After irradiation, clear liquid was obtained was used to judge at wavelength of 466 nm by a UV-vis spectrophotometer (UV-1600).

3. Results and discussion

3.1. Characterization

The crystalline phases and elemental composition of pure AgI, Ag₃BiO₃ and AgI/ABO heterojunction photocatalysts were characterized by XRD (Fig. 1). In Fig. 1, the characteristic diffraction peaks for pure Ag₃BiO₃ sample is situated at 2θ (scattering angle) about 17.2°, 24.7°, 28.3°, 33.1°, 33.6°, 34.8°, 35.7°, 38.0°, 40.1°, 46.2°, 53.0° and 58.7° assigning to the lattice planes of the (121), (321), (312), (501), (123), (242), (440), (600) (620), (253), (811) and (624),

respectively. These observed peaks match well with standard spectrum Ag_3BiO_3 (PDF no. 81-1713) which corroborates the samples synthesized. Furthermore, there no characteristic diffraction peaks could be attributed to foreign matters or other phases, the result suggests the high purity of Ag_3BiO_3 . On the other hand, as shown in Fig. 1, the principal peaks in the patterns could have an acceptable agreement with the standard spectrum of hexagonal AgI (PDF no. 09-0399). The characteristic diffraction peaks located at 2θ values of 23.7° , 39.1° , 46.3° , 56.7° , 62.3° , 71.0° and 76.1° can be assigned to the (111), (220), (311), (400), (331), (422) and (511) lattice planes of AgI structure, respectively.

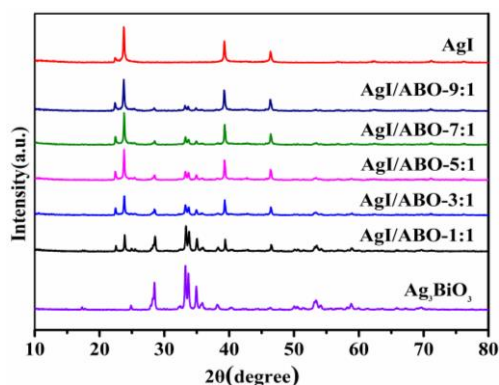


Fig. 1. XRD patterns of (a) pure AgI, (b) Ag_3BiO_3 and AgI/ABO composites.

The XRD of several AgI/ABO samples with different AgI content was also investigated, as shown in Fig. 1. According to their standard diffraction peaks, it can be seen that both Ag_3BiO_3 and AgI are identified in these samples. Moreover, with increasing the mole ratio to AgI/ABO, the peak at $2\theta = 23.7$ (the strong diffraction peak of AgI) arise and get evident increasingly. The results verified co-existence of AgI and Ag_3BiO_3 in the AgI/ABO hybrid materials.

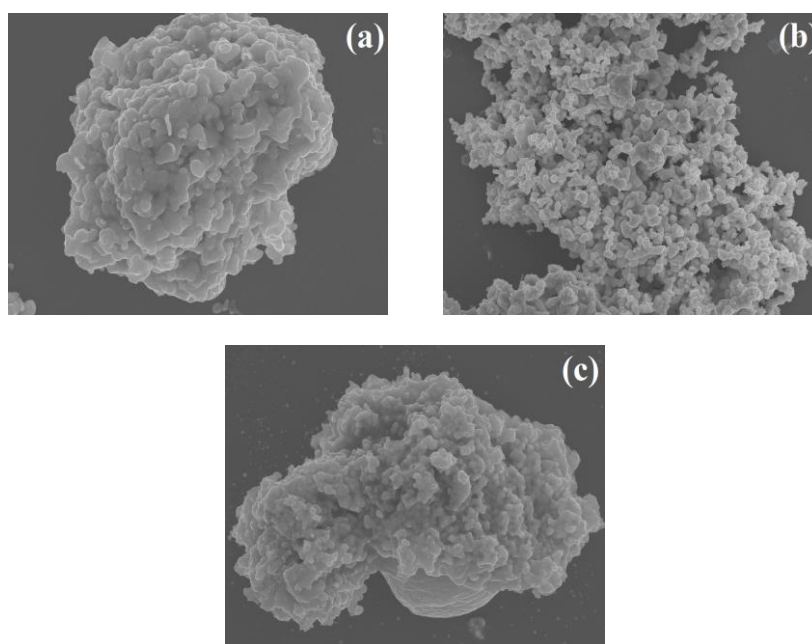


Fig. 2. SEM imagines of (a) AgI, (b) Ag_3BiO_3 and (c) AgI/ABO-5:1.

3.2. Morphology analysis

The morphology features of pure AgI, Ag_3BiO_3 and AgI/AFO-5:1 are analyzed by SEM analysis (Fig. 2). Shown in Fig. 2(a), AgI shows glossy and irregular particle. The hydrothermally grown Ag_3BiO_3 nanosheets is a nanoparticle ranged from 200 to 400 nm (Fig. 2(b)). Combined with the SEM image of pure AgI and Ag_3BiO_3 , it can be clearly see that AgI inlay with the layer Ag_3BiO_3 to form a heterojunction structure composites. It proved that a heterojunction in AgI/ABO can promote the separation and transport efficiency of electron-holes, and enhanced the photocatalytic performance.

3.3. EDS analysis

As can be seen in Fig. 3, the elemental composition was determined by EDS, which were detected on the AgI/ABO-5:1 composites sample. It illustrates independent peaks for silver (Ag), oxygen (O), cadmium (Bi) and sulfur (I) species, which suggested Ag_3BiO_3 and AgI were obtained successfully.

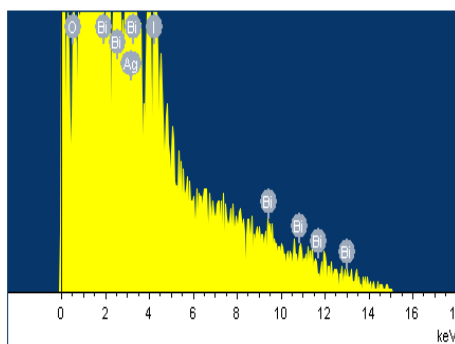


Fig. 3. The EDS patterns of AgI/ABO composite.

Furthermore, in order to investigate elements dispersion, EDS dot-mapping micrographs together with SEM image of region of study were shown in Fig. 4(a)-(e). Compared with the SEM image, it has been confirmed that the Bi and O elements, which are the elements from Ag_3BiO_3 , and the Ag element from AgI and Ag_3BiO_3 , but I element from AgI. This result is in line with SEM results of AgI/ABO-5:1 sample which have non-uniform morphology. Furthermore, considering results of XRD, SEM and EDS dot-mapping, it seems that AgI is compatible with Ag_3BiO_3 . Additionally it is expected that AgI/ABO-5:1 through good physicochemical properties and heterojunction structure would lead to the improvement of charge carries separation in photocatalytic reactions.

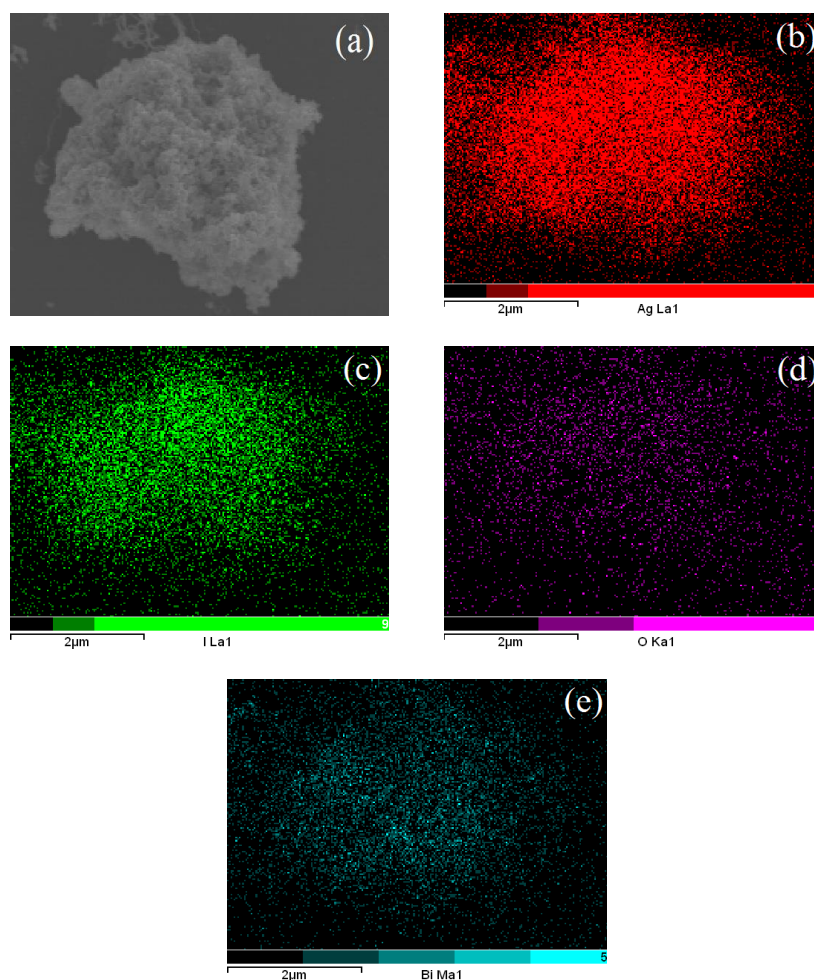


Fig. 4. EDS dot mapping analysis of synthesized nanostructured AgI/ABO-5:1 photocatalyst.

3.4. PL spectra

Fig. 5 shows the PL emission spectra of the as-prepared materials. As seen, the PL emission intensity of the AgI/ABO-5:1 is lower than that of pure Ag_3BiO_3 and AgI nanoparticles, indicating that the introduction of AgI nanoparticles can improve the charge separation. It is evidently observed that the PL intensity from the AgI/ABO-5:1 nanocomposite is significantly smaller as compared to that of the as-prepared materials. This result indicates that incorporation of AgI nanoparticles on the surface of Ag_3BiO_3 nanoparticles providing trapping sites of electrons in the band gap of Ag_3BiO_3 .

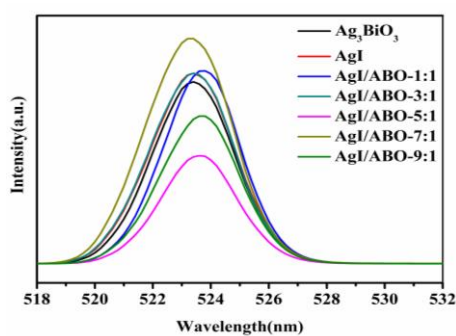


Fig. 5. PL em spectra of pure AgI, pure Ag_3BiO_3 and AgI/ABO composites.

3.5. Photocatalytic activity of photocatalyst

Under visible light irradiation, the photocatalytic activities of Ag_3BiO_3 , AgI, and AgI/ABO heterojunction were assessed by degradation of MO solution (Fig.6.). Over the pure Ag_3BiO_3 and AgI, about 14.8% and 27.4% of MO was removed for 30 min under the condition of visible light. For AgI/ Ag_3BiO_3 nanocomposites, it can be observed that the photocatalytic performance obviously increased with the incensement of AgI content. Compared to other synthesized AgI/ABO nanocomposites, AgI/ABO-5:1 sample indicates the highest photocatalytic efficiency for MO degradation, with an efficiency of 99.4% over the same time duration.

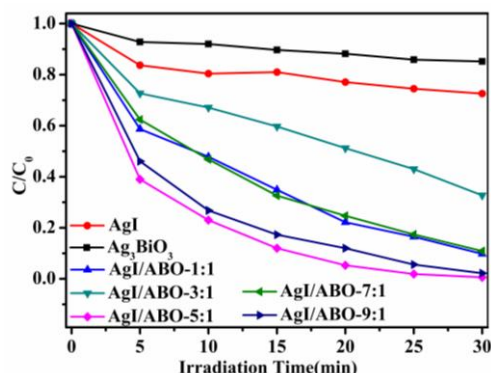


Fig. 6. Photocatalytic degradation of MO with different as-prepared photocatalyst.

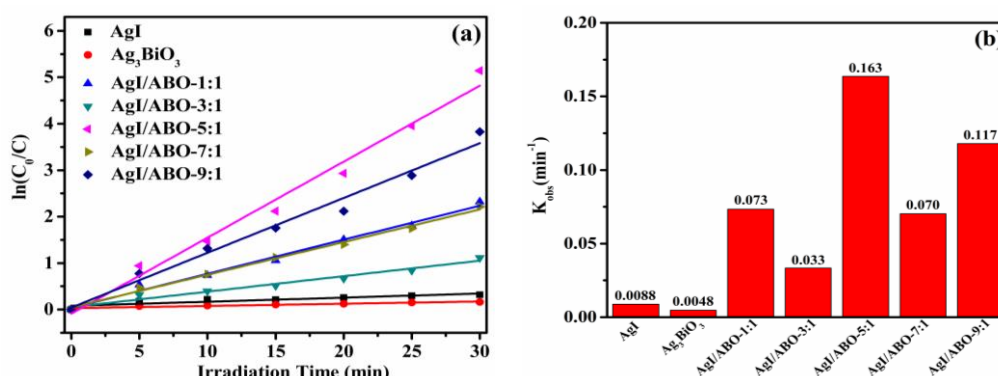


Fig. 7. (a) Photocatalytic kinetics of each process in degrading MO, and (b) first-order rate constant of different as-obtained samples.

Besides, in order to investigate the kinetics character of the process of photocatalysis, the reaction kinetics of the degradation is expressed by applying a first-order model as follow Eq. (1) [18-19]:

$$\ln(C_0/C) = K_{\text{obs}}t \quad (1)$$

where C_0 and C are the concentrations of MO in the degradation at times 0 and t , respectively. K_{obs} denoted the apparent first-order rate constant. The linear relationship and degradation rate constant are shown in Fig. 6 and Fig. 7, respectively. The AgI/ABO-5:1 photocatalyst showed the highest apparent reaction rate, and it suggests that the modification of AgI could efficiently improve the photocatalytic activity of the Ag_3BiO_3 photocatalyst.

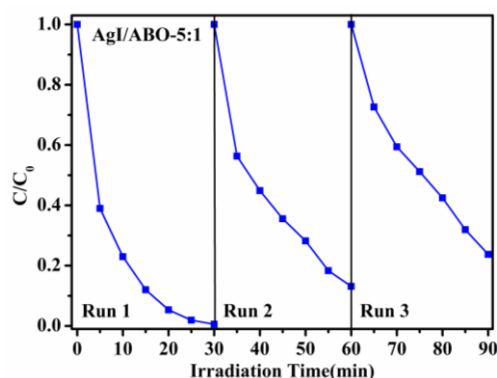


Fig. 8. Cycling runs for degradation of MO by AgI/ABO-5:1.

Fig. 8 shows the MO photodegradation kinetics by AgI/ABO-5:1 under visible light in three successive cycles. An expected decrease in photocatalytic performance from 99.4% to 76.3% was observed upon the third re-use. The decrease in performance could be assigned to washout loss of some catalyst during the recovery steps. The AgI nanoparticles loaded on the surface of Ag₃BiO₃ nanosheets can reduce dissolution in the aqueous solution, thus insuring the structural stability of AgI/ABO composite catalytic for the photocatalytic reaction. Hence, a certain amount of AgI loaded on the surface of Ag₃BiO₃ nanosheets can not only enhance the visible-light photocatalytic activity, but also insure the structure stability of AgI/ABO.

3.6. Reaction mechanism

3.6.1. Effects of reactive species

For analysed the dominant reactive species, a sequence of active species trapping tests for MO photodegradation process over the AgI/ABO-5:1 catalyst were accomplished (Fig.7). During the MO photodegradation test, superoxide radical ($\bullet\text{O}_2^-$), hydroxyl radical ($\bullet\text{OH}$) and hole (h^+) could be scavenged via adding 1mM benzoquinone (BQ), isopropanol (IPA) and ammonium oxalate (AO). After the IPA and BQ took part in the system, the photodegradation rates of MO dropped to 86% and 72% respectively. When AO participated in the degradation process, the degradation rate of MO dropped to 55% under the identical condition. On the basis of the above analyze testing data, it could be certainly concluded that superoxide radical ($\bullet\text{O}_2^-$), hydroxyl radical ($\bullet\text{OH}$) and hole ($\bullet\text{OH}$) played important roles toward MO degradation.

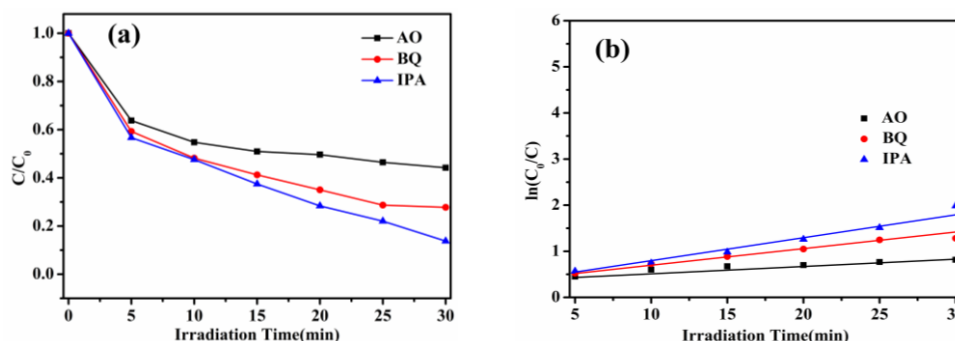
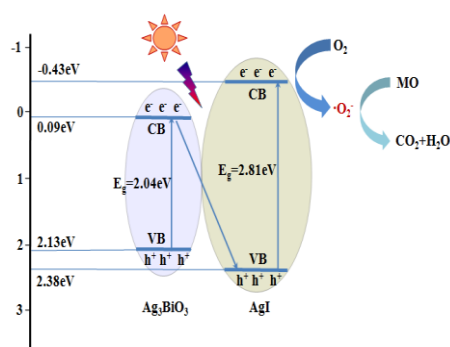
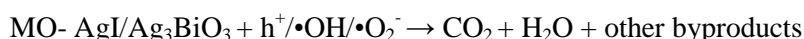
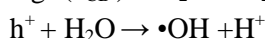
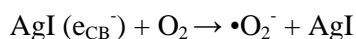
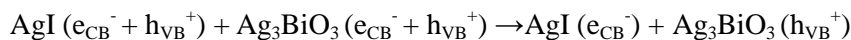


Fig. 9. (a) Photocatalytic degradation with different scavengers, (b) Photocatalytic kinetics of each process with different scavengers.

3.6.2. Photocatalytic activity enhancement mechanism of AgI/ABO composites

Based on the above experimental result, a possible mechanism of AgI/ABO hybrids was proposed for the degradation of MO dyes under solar light irradiation (Scheme 1). The possible electrons transfer process might be described as follows:



Scheme 1. The schematic possible mechanism of degradation of MO by AgI/ABO-5:1 heterostructure.

At first, under visible light, Ag_3BiO_3 and AgI can be excited to form the photoexcited holes (h^+) and electrons (e^-) in their VB and CB, respectively. Because the CB and VB of AgI are more positive than corresponding bands of Ag_3BiO_3 , the photoelectrons (e^-) photogenerated in Ag_3BiO_3 were transferred across the interface of the AgI/ABO hybrids to the surface of AgI. At the same time, the photogenerated holes (h^+) are transferred injected quickly from the VB of AgI to that of Ag_3BiO_3 , which consequently reduces the recombination of the photoexcited carriers greatly. Moreover, the CB edge potential of AgI (-0.43 eV) is more negative than the reduction potential of $\text{O}_2/\bullet\text{O}_2^-$ (-0.046 eV) [20]. The enriched electrons on the surface of AgI could be trapped by molecular oxygen in solution to form $\bullet\text{O}_2^-$. Subsequently, the MO molecules were attacked by the generated the free radicals ($\bullet\text{O}_2^-$, etc.), leading to the decolorization and opening ring reactions. Finally, the active species oxidized the dye molecules to the degradation products (CO_2 , H_2O , other byproducts.).

4. Conclusions

The AgI/ABO hybrids were grown by co-precipitation on the surfaces of hydrothermally prepared Ag_3BiO_3 to form the heterojunction nanocomposite. The as-prepared AgI/ABO composites show much higher photocatalytic activities for the degradation of MO than the pure Ag_3BiO_3 due to the matched band structure of two components and more effective charge transportation and separations. The suggested catalyst provides an effective and environmentally friendly catalyst with relatively good activity. Thus, AgI/ABO composites are very promising in the treatment of organic pollutants in wastewater.

Acknowledgments

This work was financially supported by Program of the “Provincial college students' innovation and entrepreneurship training program” (Changchun Normal University [2018062]).

References

- [1] M. Ghanbari, F. Soofivand, M. Salavati-Niasari, *Journal of Molecular Liquids* **223**, 21 (2016).
- [2] M. Cui, J. X. Yu, H.J. Lin, Y. Wu, L. H. Zhao, Y. M. He, *Appl. Surf. Sci.* **387**, 912 (2016).
- [3] H. F. Ye, H. L. Lin, J. Cao, S. F. Chen, Y. Chen, *Journal of Molecular Catalysis A: Chemical* **397**, 85 (2015).
- [4] C. S. Lei, M. Pi, X. F. Zhu, P. F. Xia, Y. Q. Guo, F. G. Zhang, *Chemical Physics Letters* **664**, 167 (2016).
- [5] Q. Wang, M. M. Chen, N. X. Zhu, X.D. Shi, H. Jin, Y. Zhang, Y. Q. Cong, *Journal of Colloid and Interface Science* **448**, 407 (2015).
- [6] H. H. Chang, J. Lv, H. C. Zhang, B. Zhang, W. L. Wei, Y. Qiao, *Biosensors and Bioelectronics* **87**, 579 (2017).
- [7] M. Rurtz, M. Jansen, *Z. Anorg. Allg. Chem.* **619**, 1446 (1993).
- [8] C. W. Li, A. C. Zhang, L. X. Zhang, J. Song, S. Su, Z. J. Sun, J. Xiang, *Appl. Surf. Sci.* **433**, 914 (2018).
- [9] J. S. Cheng, C. Wang, Y. F. Cui, Y. Sun, Y. Zuo, T. M. Wang, *Materials Letters* **127**, 28 (2014).
- [10] R. Meribout, Y. Zuo, A. A. Khodja, A. Piram, S. Lebarillier, J. S. Cheng, C. Wang, P. Wong-Wah-Chung, *Journal of Photochemistry and Photobiology A: Chemistry* **328**, 105 (2016).
- [11] L. S. Zhang, T. F. Long, C. Q. Yan, X. C. He, M. L. Cheng, S. Zhong, *Advanced Materials Research* **662**, 372 (2013).
- [12] J. Liang, G. Q. Zhu, P. Liu, C. Xu, *Journal of Nanoscience and Nanotechnology* **14**, 4185 (2014).
- [13] B. Zhang, X. Wang, Y. L. Zhao, J. Lv, H. Y. Meng, H. H. Chang, H. Zhang, W. L. Wei, *Talanta* **167**, 111 (2017).
- [14] W. Wu, X. M. Lv, J. X. Wang, J. M. Xie, *Journal of Colloid and Interface Science* **496**, 434 (2017).
- [15] S. Q. Huang, Y. G. Xu, M. Xie, Q. Q. Liu, H. Xu, Y. Zhao, M. Q. He, H. M. Li, *RSC Adv.* **7**, 30845 (2017).
- [16] J. S. Xie, C. Fang, J. J. Zou, H. D. Lu, C. G. Tian, C. L. Han, D. F. Zhao, *Materials Letters* **170**, 62 (2016).
- [17] W. Zhang, L. Zhou, J. Shi, H. P. Deng, *Journal of Colloid and Interface Science* **496**, 167 (2017).
- [18] G. Elango, S. M. Roopan, *J. Photochem. Photobio.* **155**, 34 (2016).
- [19] A. Phuruangrat, A. Maneechote, P. Dumrongrojithanath, N. Ekthammathat, S. Thongtem, T. Thongtem, *Materials Letters* **159**, 289 (2015).
- [20] Y. N. Lin, R. X. Wang, Z. K. Yang, H. Du, Y. F. Jiang, C. C. Shen, K. Liang, A. W. Xu, *Chin. J. Catal.* **36**, 2135 (2015).